Evaluation of Methods for Ridge and Valley Detection

Antonio M. López, Felipe Lumbreras, Joan Serrat, and Juan J. Villanueva, *Member, IEEE*

Abstract—Ridges and valleys are useful geometric features for image analysis. Different characterizations have been proposed to formalize the intuitive notion of ridge/valley. In this paper, we review their principal characterizations and propose a new one. Subsequently, we evaluate these characterizations with respect to a list of desirable properties and their purpose in the context of representative image analysis tasks.

Index Terms—Creases, separatrices, drainage patterns, comparative analysis.

1 Introduction

The flow of water over the Earth's surface develops an arrangement of ramified dry channels that form the so-called *drainage pattern*, which is of high interest in the field of Hydrology. Accordingly, from the last century, researchers have tried to characterize it mathematically, prompting a fruitful debate [3], [2], [19], [12], [26]. As a result, other interesting geometric entities were defined and later adopted for image analysis, the field in which the debate has followed [13], [24]. From now on, we will term the drainage patterns and any approximation to them as *valleys*. By *ridges* we will refer to the valleys of the inverted relief.

In image analysis, the ridge/valley characterizations must be evaluated with regards to their usefulness in specific applications. This paper assesses the merits of the main characterizations by testing them in several types of image analysis problems. In Section 2, we classify and review the most widespread characterizations. In Section 3, we introduce a new *ridgeness/valleyness* measure that will be shown to outperform existing ones. In Section 4, we propose a set of desirable properties that ridge/valley detectors should possess, and we present the types of applications in which ridges/valleys are usually required. Section 5 evaluates the different ridge/valley methods in the context of the proposed properties and applications. Finally, in Section 6 we draw the main conclusions.

2 Characterizing Ridges and Valleys

Firstly, some notation. $L : \Omega \subset \mathbb{R}^d \rightarrow \Gamma \subset \mathbb{R}$ will always denote a d dimensional function and $J_n[L] = \{\partial^j L / \partial i_1 \ldots \partial i_j\}_{j=0}^{n}$ its *local jet* of order n, where $\forall k \in \mathcal{I}_j : i_k \in \mathcal{X}_d$, $\mathcal{I}_j$ being a set of integer indices from 1 to j and $\mathcal{X}_d = \{x^1, \ldots, x^d\}$ the coordinate system. We also define the operators $\nabla = (\partial/\partial x^1, \ldots, \partial/\partial x^d)$ and $\nabla\nabla = (\nabla^t \cdot \nabla)$ to obtain the gradient and the Hessian of any function. Given any two vectors $\mathbf{v} = (v^1, \ldots, v^d)^t$ and $\mathbf{w} = (w^1, \ldots, w^d)^t$ in $\mathcal{X}_d$ coordinates, we can define the first order partial derivative of L along $\mathbf{v}$ as $L_{\mathbf{v}} = \nabla L \cdot (\mathbf{v}/\|\mathbf{v}\|)$, and the second order one along $\mathbf{v}$ and $\mathbf{w}$ as $L_{\mathbf{vw}} = (\mathbf{v}^t/\|\mathbf{v}\|) \cdot \nabla\nabla L \cdot (\mathbf{w}/\|\mathbf{w}\|)$. If $x^i \in \mathcal{X}_d$, L_{x^i} will refer to $\partial L/\partial x^i$.

We classify the different ridge/valley characterizations as:

- **Local**. When the classification of a point $\mathbf{x} \in \Omega$ as ridge/valley depends on a local test based on $J_n[L](\mathbf{x})$. We term as *creases* both the ridges and valleys defined by such a test. Some of these tests provide a degree of ridgeness/valleyness (creaseness).
- **Global**. When the classification of a point $\mathbf{x} \in \Omega$ as ridge/valley depends on image features arbitrarily far away from $\mathbf{x}$. For instance, the algorithms that divide Ω into districts by special lines called *separatrices*.
- **Multilocal**. At each point $\mathbf{x} \in \Omega$, the classification depends on the jets at points in a region of influence, which can be a predefined neighborhood, or can depend on the particular geometry of the image. This last case includes the drainage patterns.

2.1 Creases

Saint-Venant identified ridges/valleys in 2D as loci of minimum gradient magnitude along the relief's level curves [3]. This condition was later reformulated by Haralick [13], [10] as loci of extremal height of L in the direction along which L has the greatest magnitude of its second order directional derivative. Haralick's idea is extended to d dimensional images in [5] under the name of *height condition*. If $|\lambda_1| \geq \ldots \geq |\lambda_d|$ are the eigenvalues of $\nabla\nabla L$ and $\mathbf{v}_1, \ldots, \mathbf{v}_d$ their corresponding eigenvectors, then a nD crease ($1 \leq n \leq d$) is characterized as:

$$\forall i \in \mathcal{I}_{d-n} \; \nabla L \cdot \mathbf{v}_i = 0$$

and

$$\begin{cases} \lambda_i < 0 \text{ if ridge} \\ \lambda_i > 0 \text{ if valley}. \end{cases} \tag{1}$$

• *The authors are with The Computer Vision Center and Computer Science Department, Universitat Autònoma de Barcelona, Edifici O, 08193 Cerdanyola, Spain. E-mail: {antonio, felipe, joans, villanueva}@cvc.uab.es.*

Manuscript received 2 Mar. 1998; revised 16 Nov. 1998.
Recommended for acceptance by K. Bowyer.
For information on obtaining reprints of this article, please send e-mail to: tpami@computer.org, and reference IEEECS Log Number 107628.

In 2D, ridges/valleys have been also identified [7], [29] as positive maxima/negative minima of the curvature of the relief's level curves, κ. These maxima are connected from one level to the next, forming a subset of the so-called *vertex curves*. In d dimensions we generalize the level curves of L to *level sets*. A level set of L consists of the set of points $S_l = \{\mathbf{x} \in \Omega : L(\mathbf{x}) = l\}$ for a given constant l. Then, if $|\kappa_1| \geq \ldots \geq |\kappa_d|$ are the principal curvatures of the level hypersurface S_l and $\mathbf{t}_1, \ldots, \mathbf{t}_d$ their corresponding principal directions, a nD crease ($1 \leq n \leq d$) is characterized as (adapted from [5]):

$$\forall i \in \mathcal{I}_{d-n} \ \nabla\kappa_i \cdot \mathbf{t}_i = 0$$

and

$$\begin{cases} \mathbf{t}_i^{\mathrm{t}} \cdot \nabla\nabla\kappa_i \cdot \mathbf{t}_i < 0 \text{ and } \kappa_i > 0 \text{ if ridge} \\ \mathbf{t}_i^{\mathrm{t}} \cdot \nabla\nabla\kappa_i \cdot \mathbf{t}_i > 0 \text{ and } \kappa_i < 0 \text{ if valley}. \end{cases} \quad (2)$$

The 2D vertex condition "positive maxima/negative minima of κ" can be translated to "high values of $|\kappa|$" where $\kappa > 0$ measures ridgeness and $\kappa < 0$ valleyness. In 2D as well, when the height condition holds, we have $\mathbf{v}_1 = \mathbf{v}$ and $\lambda_1 = \mathrm{L}_{\mathbf{vv}}$, where $\mathbf{v} = (L_y, -L_x)^{\mathrm{t}}$ is the tangent vector of the level curves of L. Then, $L_{\mathbf{vv}}$ can be seen as a creaseness measure: if $L_{\mathbf{vv}}$ is high, then there are more chances that the highest value in magnitude of the second order directional derivative is reached along $\mathbf{v}$. The measures $L_{\mathbf{vv}}$ and κ are related by

$$\kappa = -L_{\mathbf{vv}} \,/\, L_{\mathbf{w}} = (2L_xL_yL_{xy} - L_y^2L_{xx} - L_x^2L_{yy})/(L_x^2 + L_y^2)^{3/2}, \quad (3)$$

where $\mathbf{w} = (L_x, L_y)^{\mathrm{t}}$ is the 2D gradient vector of L. In this way, $L_{\mathbf{vv}}$ can be considered as the measure κ weighted by the gradient magnitude in order to nullify its response at isotropic regions. However, this is a tradeoff since $L_{\mathbf{w}}$ is also lower on the center of a ridge/valley region than it is on its boundary. In [18] the family of operators $L_{\mathbf{vv}}L_{\mathbf{w}}^{\alpha}$, $-1 \leq \alpha \leq 0$ was defined, where α controls the tradeoff. The same authors defined the 3D operators $L_{\mathbf{pp}}L_{\mathbf{w}}^{\alpha}$ (ridgeness if negative) and $L_{\mathbf{qq}}L_{\mathbf{w}}^{\alpha}$ (valleyness if positive), where $\mathbf{p}$ and $\mathbf{q}$ are the principal directions of the level surfaces and, in this case, $\mathbf{w} = (L_x, L_y, L_z)^{\mathrm{t}}$.

2.2 Separatrices

Let us call *slopelines* the curves that follow the landscape gradient direction. In 2D, Maxwell [19] defined *basins* as districts whose slopelines come from the same minimum, and *hills* as districts whose slopelines reach the same maximum. He called *watersheds* the slopelines dividing a landscape into basins, and *watercourses* the ones dividing it into hills. These watersheds/watercourses were supposed to coincide with the ridges/valleys previously defined by Cayley [2] as slopelines going from maximum/minimum to maximum/minimum through a saddle point. However, the slopeline going from maximum to maximum is a watershed only if the two maxima are different points (analogously for minima and watercourses). If not, the slopelines are called *virtual separatrices* which, together with the watersheds/watercourses, form the *separatrices* of the landscape [8].

More recent work has brought separatrices as a tool for image analysis [20], [9], [25]. Special attention should be paid to the efficient algorithms presented in [30], [1] to extract the watersheds of a d dimensional image, which, although designed for discrete spaces, "converge" on the definition in the continuous domain [21]. They are based on an immersion process analogy of the image landscape. In 2D, imagine we pierce each minimum of the landscape and we plunge the landscape into a lake with a constant vertical speed. The water entering through the holes floods the landscape's surface. During the flooding, two or more floods coming from different minima may merge. We want to avoid this event, and we build a dam on the points of the surface where the floods would merge. At the end of the process, only the dams emerge and they constitute the watershed of the landscape. Watercourses are obtained by applying this algorithm to the inverted image.

2.3 Drainage Patterns

Some authors [13] affirm that the proper mathematical characterization of the drainage patterns is due to R. Rothe, although others do not agree [24]. In an idealized landscape, the water flows downhill along slopelines (steepest slope routes). Therefore, Rothe [26] identified valleys as (parts of) slopelines where others converge to form a channel stream and eventually join in a minimum (maybe at infinity). On the other hand, researchers working with real topographic data such as digital elevation models (DEMs) [22], [4] extract drainage patterns directly by simulating the flow of water over the Earth's surface, known as *runoff*. After the simulation, drainage lines of different relevance are identified by their water accumulation.

An efficient simulator for 2D images can be found in [27]. It relies on first eliminating all the local minima and the planar areas to ensure the continuity of streamlines. Then, the initial accumulation at each pixel is set to one. Next, the runoff is simulated by ordering the pixels in decreasing height, and following the ordered sequence by traveling from each pixel to its neighbor with the lowest height, adding the accumulation of the previous pixel to the next.

3 Multilocal Creaseness

In [16] we reported that operators such as κ, $L_{\mathbf{vv}}$, $L_{\mathbf{pp}}$, and $L_{\mathbf{qq}}$ give rise to discontinuities at places where we do not expect any meaningful reduction of creaseness because they are the center of elongated grey-level objects, that is, at places that have a qualitatively similar anisotropic distribution of intensities to other points where these operators work well. We argued that the problem comes from their very local nature. Therefore, we proposed several new creaseness measures based on a multilocal approach. The details of how these measures were designed and the study of their properties are beyond the scope of this paper and can be found in [15]. However, since all the creaseness measures described in Section 2.1 are local, we thought that it would be interesting to include one of these new multilocal operators in the comparative evaluation of this paper. We describe briefly the one based on the so-called *structure tensor*.

Let $\mathbf{w}(\mathbf{x}) = (L_{x^1}(\mathbf{x}), \ldots, L_{x^d}(\mathbf{x}))^{\mathrm{t}}$ be the gradient vector of L at $\mathbf{x} \in \Omega$, and $G(\mathbf{x}; \sigma)$ the d-dimensional Gaussian of standard deviation σ, centered at $\mathbf{x}$. We define the structure tensor at $\mathbf{x}$ as the following symmetrical and semipositive definite $d \times d$ matrix [11]:

$$\mathbf{S}(\mathbf{x}; \sigma_{\mathrm{I}}) = G(\mathbf{x}; \sigma_{\mathrm{I}}) * (\mathbf{w}(\mathbf{x}) \cdot \mathbf{w}^{\mathrm{t}}(\mathbf{x})) , \quad (4)$$

where the convolution "*" of the matrix $(\mathbf{w}(\mathbf{x}) \cdot \mathbf{w}^{\mathrm{t}}(\mathbf{x}))$ with the Gaussian is element-wise. The parameter σ_{I} is the *integration scale* and, if $\mathbf{w}'(\mathbf{x}; \sigma_{\mathrm{I}})$ is the eigenvector corresponding to the largest eigenvalue of $\mathbf{S}(\mathbf{x}; \sigma_{\mathrm{I}})$, then the dominant gradient vector in a neighborhood of Ω centered at $\mathbf{x}$ and of size proportional to σ_{I} is:

$$\tilde{\mathbf{w}}(\mathbf{x}; \sigma_{\mathrm{I}}) = \mathrm{sign}\,(\mathbf{w}'^{\mathrm{t}}(\mathbf{x}; \sigma_{\mathrm{I}}) \cdot \mathbf{w}(\mathbf{x}))\mathbf{w}'(\mathbf{x}; \sigma_{\mathrm{I}}) . \quad (5)$$

The structure tensor analysis assumes that every point has a preferred orientation, which can be checked by a confidence measure: for each orientation we associate a value $\mathsf{C} \in [0, 1]$, which can be computed from the eigenvalues of $\mathbf{S}(\mathbf{x}; \sigma_{\mathrm{I}})$, say $\lambda_1(\mathbf{x}; \sigma_{\mathrm{I}}) \geq \ldots \geq \lambda_d(\mathbf{x}; \sigma_{\mathrm{I}}) \geq 0$. Similarity of the eigenvalues implies isotropy and, as a result, C should be close to zero. A suitable function for an experimentally chosen c is:

$$\mathsf{C}(\mathbf{x}; \sigma_{\mathrm{I}}) = 1 - e^{-\left(\sum_{i=1}^{d}\sum_{j=i+1}^{d}(\lambda_i(\mathbf{x};\sigma_{\mathrm{I}})-\lambda_j(\mathbf{x};\sigma_{\mathrm{I}}))^2\right)^2 / 2c^2} . \quad (6)$$

Now, in d dimensions, let C be a $(d-1)$-dimensional simple closed boundary of a neighborhood centered at a point $\mathbf{x}$, let $\mathbf{n}$ be the unitary normal vector of C and $d\ell$ the $(d-1)$-dimensional volume element of C (e.g., Fig 1a depicts the 2D continuous case). Accordingly, we define the multilocal creaseness measure $\tilde{\kappa}_d$ at $\mathbf{x}$ as:

$$\tilde{\kappa}_d = -\int_{\mathbf{y}\in C} \tilde{\mathbf{w}}^{\mathrm{t}}(\mathbf{y}; \sigma_{\mathrm{I}}) \cdot \mathbf{n}(\mathbf{y})\, d\ell . \quad (7)$$

The multilocality nature of $\tilde{\kappa}_d$ is due to the boundary C and the parameter σ_{I}. The effect of increasing C or σ_{I} is described in [15].

The discretization of $\tilde{\kappa}_d$ can be stated as follows. Let $\mathcal{B} = \{\mathbf{x}_1, \ldots, \mathbf{x}_r\}$ be the set of points that form the discrete boundary C of a neighborhood centered at $\mathbf{x}$, and let $\mathcal{U} = \{\tilde{\mathbf{w}}_1, \ldots, \tilde{\mathbf{w}}_r\}$ be a set of vectors such that $\forall k \in \mathcal{I}_r$: $\tilde{\mathbf{w}}_k = \tilde{\mathbf{w}}(\mathbf{x}_k; \sigma_{\mathrm{I}})$, for a given σ_{I}. Then, according to (7) and after a useful rescaling, $\tilde{\kappa}_d$ can be discretized as:

$$\tilde{\kappa}_d = -\frac{d}{r}\sum_{k=1}^{r} \tilde{\mathbf{w}}_k^{\mathrm{t}} \cdot \mathbf{n}_k , \quad (8)$$

$\mathcal{N} = \{\mathbf{n}_1, \ldots, \mathbf{n}_r\}$ being the set of unit normal vectors to C at each boundary site, that is, $\forall k \in \mathcal{I}_r : \mathbf{n}_k = \mathbf{n}(\mathbf{x}_k)$. The simplest case is in 2D ($d = 2$) with $\mathcal{B}$ composed of the four nearest neighbors of each pixel ($r = 4$). That is, for the pixel $p_{i,j}$ of coordinates $[i, j]$ we have $\mathcal{B} = \{p_{i,j-1}, p_{i+1,j}, p_{i,j+1}, p_{i-1,j}\}$ and $\mathcal{N} = \{\mathbf{n}_{\mathrm{N}}, \mathbf{n}_{\mathrm{E}}, \mathbf{n}_{\mathrm{S}}, \mathbf{n}_{\mathrm{W}}\}$, according to the scheme of Fig. 1b. Therefore, at $p_{i,j}$ we have:

$$\tilde{\kappa}_2[i, j] = -\frac{1}{2}(\tilde{w}^1[i+1, j] - \tilde{w}^1[i-1, j] + \tilde{w}^2[i, j+1] - \tilde{w}^2[i, j-1]) , \quad (9)$$

where $\tilde{\mathbf{w}} = (\tilde{w}^1, \tilde{w}^2)^{\mathrm{t}}$. From now on, we denote $\tilde{\kappa}_2$ according to (9), as $\tilde{\kappa}^{\diamond}$ where the symbol "$\diamond$" recalls the shape of C. The 3D equivalent ($d = 3$) uses the six nearest neighbors of each voxel ($r = 6$) to form $\mathcal{B}$. That is, for the voxel $p_{i,j,k}$ and according to the scheme of Fig. 1c, we have $\mathcal{B} = \{p_{i,j-1,k}, p_{i+1,j,k}, p_{i,j+1,k}, p_{i-1,j,k}, p_{i,j,k-1}, p_{i,j,k+1}\}$ and $\mathcal{N} = \{\mathbf{n}_{\mathrm{N}}, \mathbf{n}_{\mathrm{E}}, \mathbf{n}_{\mathrm{S}}, \mathbf{n}_{\mathrm{W}}, \mathbf{n}_{\mathrm{F}}, \mathbf{n}_{\mathrm{B}}\}$. Then at $p_{i,j,k}$:

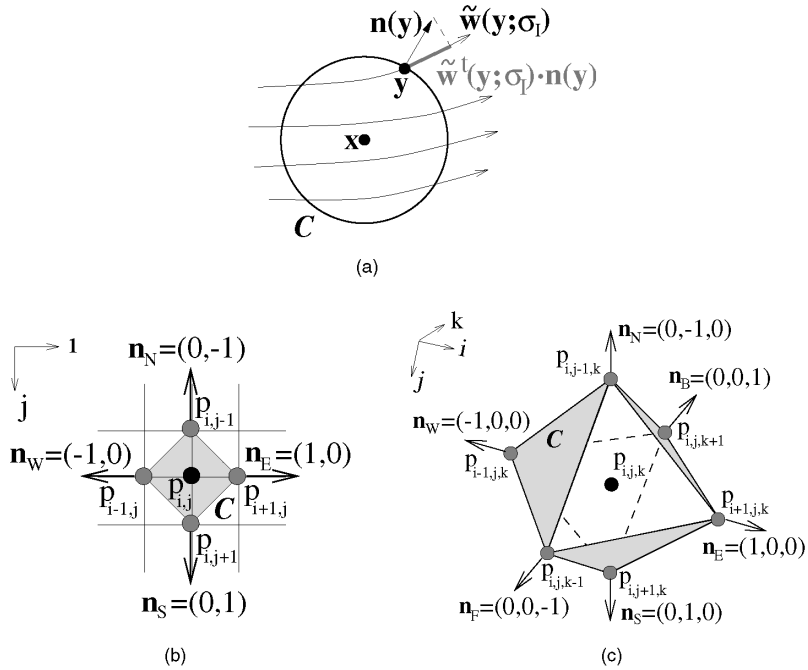

Fig. 1. (a) Geometry involved in the definition of $\tilde{\kappa}_d$ at $\mathbf{x}$ in the continuous domain, for $d = 2$; (b) boundary C on a 2D regular grid according to the four nearest neighbors; (c) The same in 3D for the six nearest neighbors.

$$\tilde{\kappa}_3[i, j, k] = -\frac{1}{3}\big(\tilde{w}^1[i+1, j, k] - \tilde{w}^{-1}[i-1, j, k] + \tilde{w}^2[i, j+1, k] - \tilde{w}^2[i, j-1, k] + \tilde{w}^3[i, j, k+1] - \tilde{w}^3[i, j, k-1]\big), \quad (10)$$

where $\tilde{\mathbf{w}} = (\tilde{w}^1, \tilde{w}^2, \tilde{w}^3)^t$. From now on, we denote $\tilde{\kappa}_3$ according to (10) as $\tilde{\kappa}_M^{\diamond}$.

It is easy to show [15] that in d dimensions $|\tilde{\kappa}_d| \le d$. Moreover, $|\tilde{\kappa}_d|$ approaches the codimension of the ridges and valleys to and from which the vector field $\tilde{\mathbf{w}}$ converge and diverge. This gives us a reasonable way to threshold $\tilde{\kappa}_d$ in order to extract creases too. In addition, since $C \in [0, 1]$ we can use the measure $C\tilde{\kappa}_d$ to get rid of creaseness at isotropic or background regions, and still keep the same bounds of $\tilde{\kappa}_d$ up.

4 Criteria for Evaluating Ridge/Valley Algorithms

In order to assess the validity of the different ridge/valley characterizations, we have devised a set of desirable properties referring to the clean (**P1**–**P4**) and robust (**P5**, **P6**) extraction of salient ridges/valleys:

P1. *No over-detection*. Irrelevant ridges/valleys should not be detected.

P2. *No under-detection*. Salient ridges/valleys must always be detected.

P3. *Continuity*. Continuous ridges/valleys must be obtained from a continuous object.

P4. *Good contrast*. A creaseness measure should have a much higher value on a crease than around it and should maintain a similar value along the crease.

P5. *Structural stability*. Small perturbations of the image should not greatly alter the shape or the location of the ridges/valleys.

P6. *Good localization*. Ridges/valleys should run as closely as possible through the center of anisotropic objects.

It is difficult to quantify these properties because their practical relevance depends on the application. Therefore, we will comment on them in the context of the following types of applications, to which most specific applications using ridges/valleys belong:

T1 *Extraction of medial axes*. These applications are those in which we need to extract the central axes of an anisotropic grey-level object. In this context we present a specific application on which we are currently working: the delineation of the main stream of the right coronary artery (RCA) from 2D coronary arteriographies (Fig. 2a), with the purpose of collecting spatio-temporal understanding of the cardiovascular dynamics.

T2 *Medialness approximation*. This consists of determining how closely a point is from a central axis of an anisotropic grey-level object. We are working on the registration of CT and MR brain volumes [14] from the same patient, which is useful because CT depicts bone accurately while MR depicts better the soft tissues (Fig. 3a and 3d). Our method is similar to van den Elsen's [6]: the registration is achieved by aligning a ridgeness measure, computed from the CT, with a valleyness measure computed from the MR, both tuned to be high only on the center of the skull (medialness). Since the skull is undeformable, only rigid transformations need to be assessed. The matching quality of a transform is given by the correlation between ridgeness and valleyness.

T3 *Segmentation*. In many applications, homogeneous objects are separated by narrow ridges/valleys, therefore, their delineation segments the objects. An example is our work on the segmentation of marble grains [17]. Microscope images of thin marble sections (Fig. 4a) are used to determine the geographical origin of the marble. The classification is based on the shape, size and spatial distribution of the marble grains, which can be segmented by delineating the narrow valleys that separate them.

T4 *Extraction of drainage patterns*. The delineation of the true paths of the Earth's surface along which water gathers to run downhill, e.g., from DEMs (Fig. 5a), is of high interest in civil engineering as well as in water management.

The specific applications from the types **T1**, **T3**, and **T4** require ridge/valley delineation in 2D while the applications of type **T2** require a 3D ridgeness/valleyness measure.

5 Evaluation

For the applications in 2D we will take into account the height and vertex conditions, the $L_{\mathbf{vv}}$, κ, and $C\tilde{\kappa}^{\diamond}$ operators, watercourses, and drainage patterns. For the application in 3D we will compare $L_{\mathbf{pp}}$, $L_{\mathbf{qq}}$, and $C\tilde{\kappa}_M^{\diamond}$. For each application we will comment on the main problems of these ridge/valley characterizations with regards to the properties described in the previous section.

5.1 Implementation Details and Parameter Selection

Derivatives for creases and creaseness were obtained as finite centered differences of a smoothed version of the original image. In fact, we tested other approaches (Gaussian derivatives and derivatives of fitting polynomials) and found very similar final results. Smoothing was performed by convolving the image with a Gaussian kernel whose standard deviation, namely the *differentiation scale* σ_D, was manually tuned to yield the best output. For the image in Fig. 2a we used $\sigma_D = 4$ pixels, as well as for the CT and MR volumes of Fig. 3a and 3d. For Figs. 4a and 5a we used $\sigma_D = 2$ pixels, except in the case of the vertex condition of Fig. 4d which needed $\sigma_D = 4$ pixels to give a reasonable output.

The height and vertex conditions were checked in 2D by looking for sign changes in their corresponding zero-crossing functions in a raster manner. Both pixels involved in a change of sign were labeled as satisfying the condition. Afterwards, a thinning algorithm was used to obtain 1-pixel-wide lines.

Creases can be also obtained by thresholding a creaseness measure. With κ and $L_{\mathbf{vv}}$ we tuned the threshold value to obtain the best output in each application. With $\mathsf{C}\tilde{\kappa}^{\diamond}$ we used the same value in all the applications, due to its well defined dynamic range. However, each application required its own constant c to compute C since it depends on the contrast of the objects we are looking for. Despite of this, a fine tuning was not required. Finally, we also thinned the thresholded image to obtain 1-pixel-wide lines.

To extract watercourses, we implemented the algorithm proposed by Beucher and Meyer [1], briefly described in Section 2.2. As the authors suggest, we apply an erosion-reconstruction morphological filtering to remove spurious local maxima, prior to watercourse extraction. The amount of filtering was manually tuned for each application, in order to achieve the best result. In Fig. 2g we use a black line to represent the watercourse obtained for a severe filtering, and a lighter grey value to represent the watercourses obtained with a slight filtering. In Fig. 5g we did the opposite for the sake of visualization.

The drainage pattern algorithm we have chosen is from [27], briefly described in Section 2.3. In Fig. 2h the drainage pattern is shown as lines of different grey values depending on the amount of accumulated water, the darker the greater the accumulation is, and therefore the higher the line relevance. For the sake of visualization, in Figs. 4h and 5h the criterion is the opposite.

5.2 Results Evaluation

Delineation of the RCA centerline from coronary arteriographies. The ridge/valley detection based on vertex condition (Fig. 2d) is unsatisfactory, due to the high number of irrelevant branches joining the main centerline (**P1** fails). Some of these branches are artifacts due to the high order of the derivatives involved in the vertex condition. Thresholding of κ or $L_{\mathbf{vv}}$ (Fig. 2b and 2c) does not suffer from this problem, but the obtained centerline has many discontinuities (**P3** fails). Thresholding $\mathsf{C}\tilde{\kappa}^{\diamond}$ produces a quite continuous and clean centerline (Fig. 2e). The output of the height condition (Fig. 2f) is similar to the one of $\mathsf{C}\tilde{\kappa}^{\diamond}$ since, in this case, the value of the extrema of the second order directional derivative contributed to discard points where this value is too low, otherwise background lines would appear as with κ. The obtained RCA centerline is continuous, although it contains some spurious branches.

In Fig. 2g we can see the watercourses. With a slight filtering, we obtained a myriad of regions so that some of their borders cover the RCA centerline (**P1** fails). With a stronger filtering only the black line along the RCA in Fig. 2g is detected, which fails to delineate the final part of the RCA (**P6** fails). Furthermore, the detection of this line was found to be very unstable along a whole sequence of arteriographies (**P2** and **P5** fail).

The drainage pattern algorithm is able to extract the dark line of Fig. 2h, which runs irregularly near the center of the RCA, and suffers from under-detection in the distal of the RCA (**P2** and **P6** fail). This is mainly due to the fact that removing the local minima and planar areas implicitly modifies the shape of the image. On the other hand, without this preprocessing, the algorithm produces a poor accumulation, making it difficult to obtain a main stream. We think that by designing an intelligent method to overflow minima and planar areas, in such a way that the runoff could be simulated after a Gaussian smoothing of the original image instead of the prefiltering based on removing the local minima and planar areas, the drainage pattern would follow more precisely the center of the RCA. However, it would yet be difficult to obtain a continuous stream with high accumulation along the whole RCA center.

Due to the continuity and cleanness of the RCA centerline using $\mathsf{C}\tilde{\kappa}^{\diamond}$, we have chosen it for this application. To isolate the RCA centerline, short lines are removed, since they belong to the background. Notice that this criterion

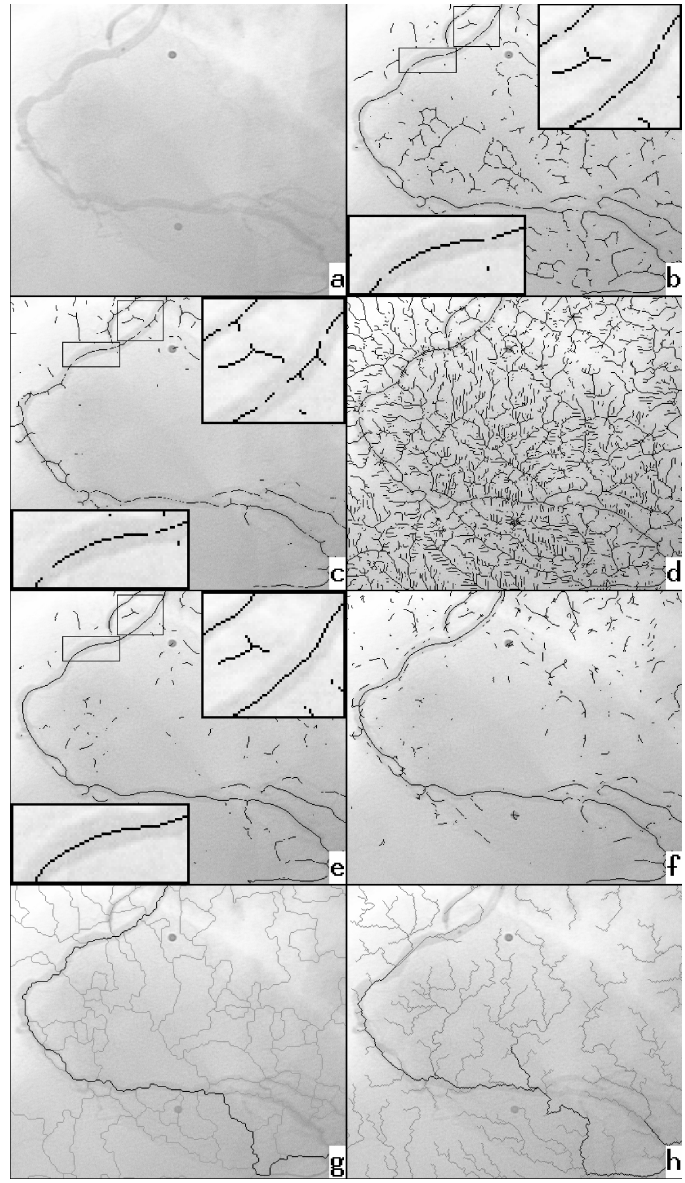

Fig. 2. (a) Coronary arteriography imaging the right coronary artery. Valleys based on (b) negative large values of κ; (c) positive large values of $L_{\mathbf{vv}}$; (d) vertex condition for valleys; (e) negative large values of $\mathsf{C}\tilde{\kappa}^{\diamond}$ (σ_{I} = 2.0 pixels and c = 0.01); (f) height condition for valleys, (g) watercourses (grey lines: after a slight filtering, black line: after a strong filtering), (h) drainage pattern.

would be useless with κ or $L_{\mathbf{vv}}$ (Fig. 2b and 2c) due to their discontinuity problems.

Registration of CT and MR brain volumes. To obtain a good matching between the ridgeness from the CT and the valleyness from the MR, we want these creaseness measures to have a high, continuous and homogeneous response along the center of the skull, and to be low elsewhere. Fig. 3 shows the results based on $L_{\mathbf{pp}}$, $L_{\mathbf{qq}}$, and $C\tilde{\kappa}^{\diamond}_{\mathrm{M}}$. Notice how both $L_{\mathbf{pp}}$ applied to the CT and $L_{\mathbf{qq}}$ to the MR present many discontinuities along the skull (**P3** fails), and they do not have a homogeneous contrast (**P4** fails). Furthermore, $L_{\mathbf{qq}}$ gives a high response in the brain, due to the sulci and the separation between the two brain hemispheres (**P1** fails). The response of $C\tilde{\kappa}^{\diamond}_{\mathrm{M}}$ is high, continuous and homogeneous along the skull center of both the CT and MR image. Furthermore, only the separation between the brain hemispheres produces extra valleyness in the MR volume. Accordingly, for this application we chose the $C\tilde{\kappa}^{\diamond}_{\mathrm{M}}$ operator.

Segmentation of marble grains. The drainage patterns (Fig. 4h) do not follow the grain boundaries (**P6** fails) as drainage lines of equal relevance (accumulation). The observation about the prefiltering done in the context of the RCA centerline delineation applies in this case too.

The κ, $L_{\mathbf{vv}}$, and $C\tilde{\kappa}^{\diamond}$ operators, and the height and vertex conditions give acceptable results (Fig. 4b, 4c, 4d, 4e, and 4f), $C\tilde{\kappa}^{\diamond}$ being the best among them. However, none of these operators ensured closed regions, unlike the case of watercourses (Fig. 4g). The response of $C\tilde{\kappa}^{\diamond}$ could be postprocessed to give such closed regions too. However, despite then having fewer regions than with watercourses (compare Fig. 4e and 4g), we still could not ensure that each one corresponds to a different grain. Therefore, in any case, we had to build an application-dependent region grouping procedure. Thus, the watershed algorithm seems to be the most suitable.

Drainage pattern delineation from DEMs. Fig. 5 shows that the best output for DEMs is given by the algorithm that simulates the overland flow of water. Since the streamlines can be ordered according to the degree of accumulation, by successive thresholds we can obtain streamlines of different relevance.

The operator $C\tilde{\kappa}^{\diamond}$ is able to detect the main lines. The κ and $L_{\mathbf{vv}}$ operators present discontinuities (**P3** fails). The height and vertex conditions also delineate the main lines but the response is noisy. The vertex condition yields more detail than the other crease operators.

The drainage patterns do not divide the landscape into closed regions, therefore, using watercourses, arbitrary lines appear and disappear (**P1** and **P2** fail).

6 Discussion

In this paper, we have classified, reviewed and compared most relevant ridge/valley characterizations: the height condition, vertex condition, $L_{\mathbf{vv}}$, κ, $L_{\mathbf{pp}}$, and $L_{\mathbf{qq}}$ from the local class, drainage patterns from the multilocal class and watercourses from the global class. The comparison has been performed by analyzing general desirable properties when applied to real 2D and 3D image analysis problems. They were chosen to be representative of the types of problems in which ridge/valley structures are commonly employed. We have included the multilocal creaseness measure $C\breve{\kappa}_d$, proposed by us, in the comparison.

In general, we think that the most suitable characterizations to approximate medial structures are crease operators. However, separatrices (e.g., watersheds) can be very useful in the event of the medial structure being a closed feature (e.g., a closed curve in 2D) and being able to devise a suitable and stable filtering process or set of markers. In comparison, drainage patterns are not appropriate for approximating such structures from grey-level images. On the other hand, we realize that none of these approaches takes into account the boundaries of the objects. Therefore, when we need to extract their medial axes very accurately, we can use the

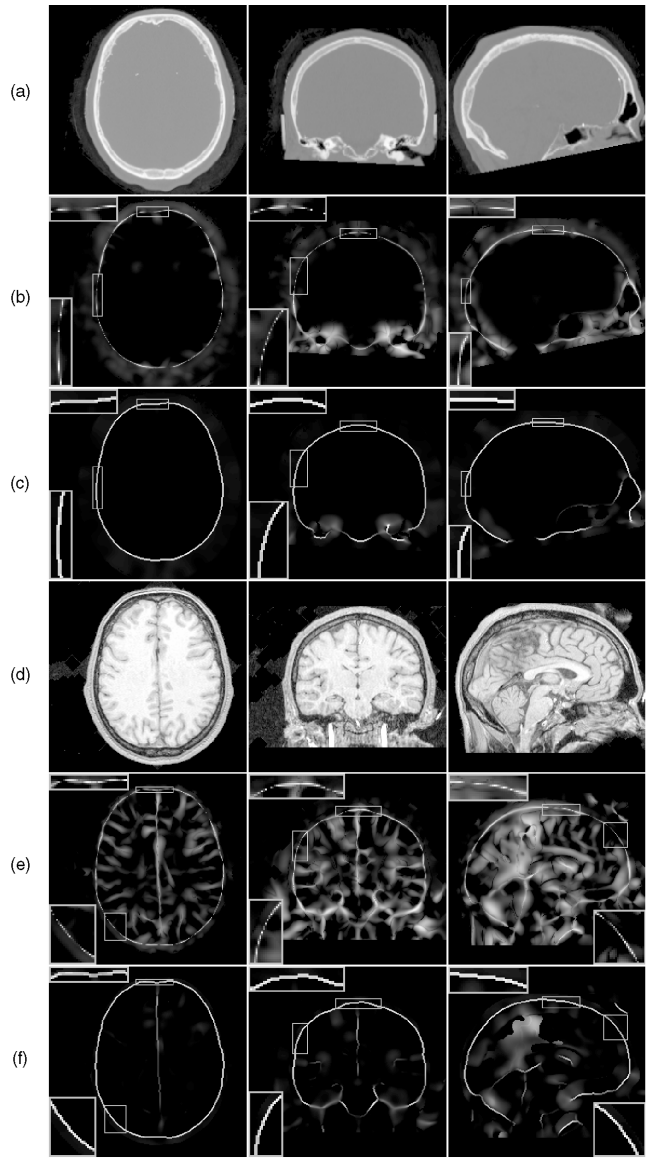

Fig. 3. From top to bottom row: (a) Transversal, coronal and sagittal slices of a CT volume with cubic voxels; (b) $L_{\mathbf{pp}}$ (negative values) of the CT; (c) $C\tilde{\kappa}^{\diamond}_{\mathrm{M}}$ (positive values) of the CT (σ_l = 4 pixels and c = 1,000); (d) Transversal, coronal and sagittal slices of a MR volume with voxels of the same size as the CT; (e) $L_{\mathbf{qq}}$ (positive values) of the MR; (f) $C\tilde{\kappa}^{\diamond}_{\mathrm{M}}$ (negative values) of the MR (σ_l = 4 pixels and c =1,000).

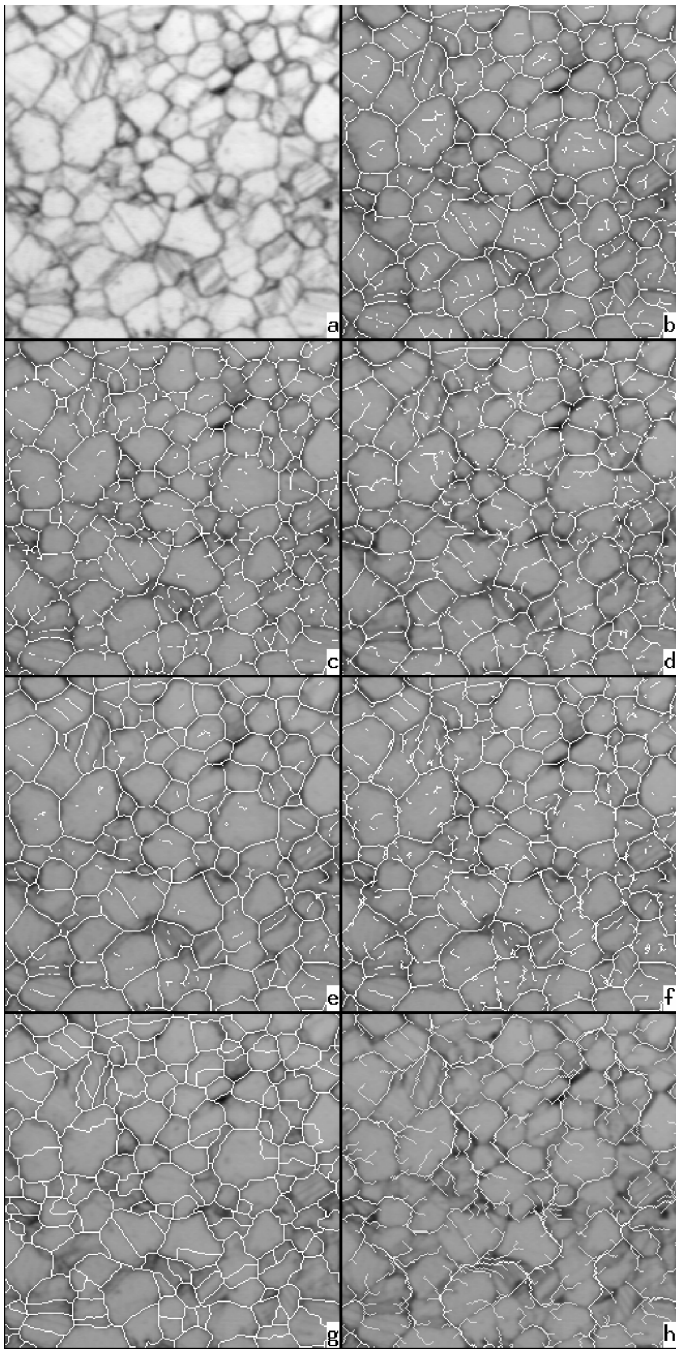

Fig. 4. (a) Petrographical microscope image of a thin marble section showing the granular structure. Valleys based on (b) negative large values of κ; (c) positive large values of $L_{\mathbf{vv}}$; (d) vertex condition for valleys; (e) negative large values of $C\tilde{\kappa}^{\diamond}$ (σ_l = 1.0 pixels and c = 1.0); (f) height condition for valleys; (g) watercourses; (h) drainage pattern.

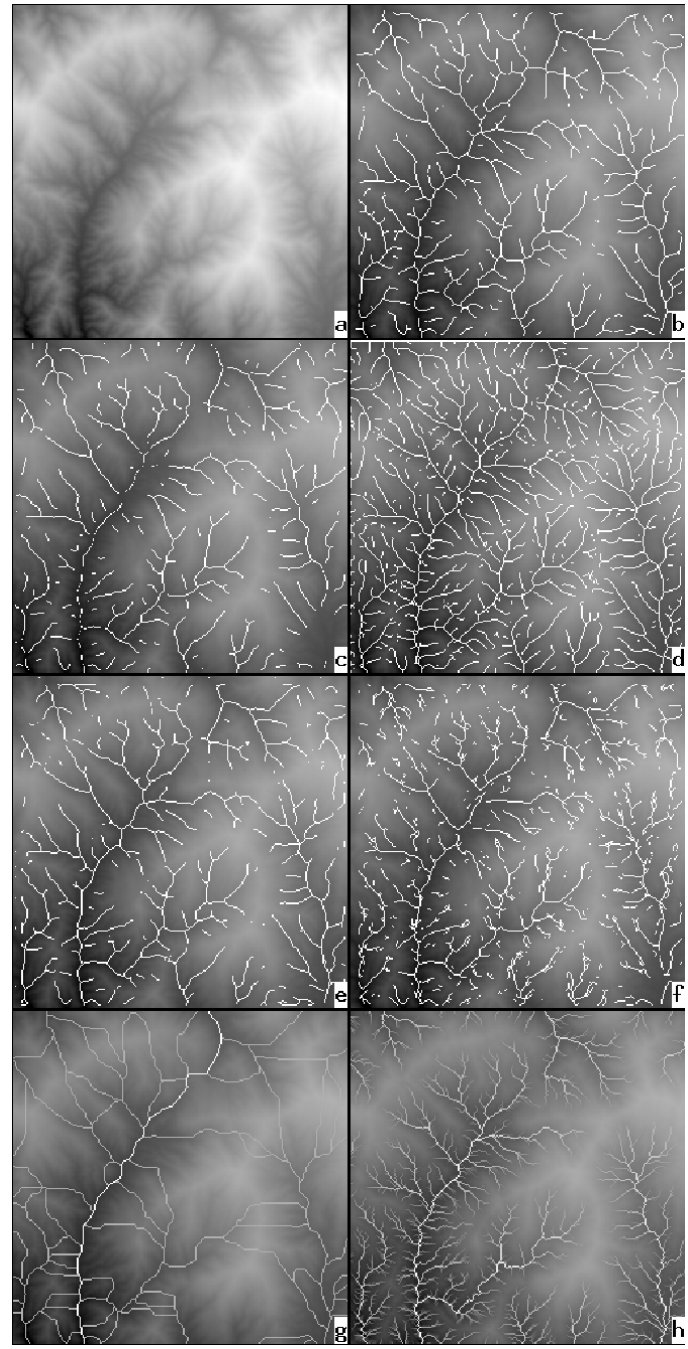

Fig. 5. (a) Digital elevation model. Valleys based on (b) negative large values of κ, (c) positive large values of $L_{\mathbf{vv}}$; (d) vertex condition for valleys; (e) negative large values of $C\tilde{\kappa}^{\diamond}$ (σ_l = 1.0 pixels and c = 1.0); (f) height condition for valleys; (g) watercourses (grey lines: after a slight filtering, white line: after a strong filtering); (h) drainage pattern.

ridges/valleys as '"initial approach" and after refine their position as is done in [28] for 2D images, or take a more sophisticated and expensive multiscale approach as in [23].

The watershed transform is, in general, the best ridge/valley method for segmentation purposes. Usually, a suitable filtering scheme to remove local minima or a reliable set of markers are mandatory. An application-dependent region merging postprocessing is also a good solution. Crease operators perform well in segmentation problems, but do not guarantee closed regions. However, they tend to produce less oversegmentation. Again, in comparison, drainage patterns do not seem too useful in extracting object boundaries.

To compute the true drainage pattern, the best algorithms are clearly those based on simulating the overland flow of water. Here we have used only one of the methods existing on the literature of image analysis and Earth sciences. Their comparison under different characteristics of

the Earth relief is out of the scope of this paper. In this direction, the work in [4] is an example. Separatrices are useless for that purpose, since drainage patterns do not divide the landscape into closed regions. Creases can eventually be used to detect relevant streams.

The height condition has proved to be more useful than the vertex condition. On the other hand, the thresholding of our creaseness measure $C\tilde{\kappa}_d$ gives better or similar results, in general, than the height condition. Furthermore, $C\tilde{\kappa}_d$ has proved to give a continuous and homogeneous creaseness, unlike κ and $L_{\mathbf{vv}}$ in 2D or $L_{\mathbf{pp}}$ and $L_{\mathbf{qq}}$ in 3D.

ACKNOWLEDGMENTS

This research was partially funded by CICYT projects TIC97-1134-C02-02 and TAP96-0629-C04-03. The authors gratefully acknowledge Dr. Petra van den Elsen from the 3D-CVG at Utrecht University for providing us with two 3D CT and MR brain datasets.

REFERENCES

[1] S. Beucher and F. Meyer, "The Morphological Approach to Segmentation: The Watershed Transform," D. Dougherty, ed., *Mathematical Morphology in Image Processing*, pp. 433–481. Marcel Dekker, Inc., 1993.

[2] A. Cayley, "On Contour and Slope Lines," *The London, Edinburgh and Dublin Philosophical Magazine and J. of Science*, vol. 18, no. 120, pp. 264–268, 1859.

[3] M. De Saint-Venant, "Surfaces à Plus Grande Pente Constituées sur des Lignes Courbes," *Bulletin de la soc. philomath. de Paris*, pp. 24–30, Mar. 1852.

[4] J. Desmet and G. Govers, "Comparison of Routing Algorithms for Digital Elevation Models and Their Implications for Predicting Ephemeral Gullies," *Int'l. J. Geographical Information Systems*, vol. 10, no. 3, pp. 311-331, Apr. 1996.

[5] D. Eberly, R. Gardner, B. Morse, S. Pizer, and C. Scharlach, "Ridges for Image Analysis," *J. Math. Imaging and Vision*, vol. 4, no. 4, pp. 353–373, Dec. 1994.

[6] P. van den Elsen, J. Maintz, E-J. Pol, and M. Viergever, "Automatic Registration of CT and MR Brain Images Using Correlation of Geometrical Features," *IEEE Trans. Medical Imaging*, vol. 14, no. 2, pp. 384–396, June 1995.

[7] J. Gauch and S. Pizer, "Multiresolution Analysis of Ridges and Valleys in Grey-Scale Images," *IEEE Trans. Pattern Analysis and Machine Intelligence*, vol. 15, no. 6, pp. 635–646, June 1993.

[8] L. Griffin and A. Colchester, "Superficial and Deep Structure in Linear Diffusion Scale Space: Isophotes, Critical Points and Separatrices" *Image and Vision Computing*, vol. 13, no. 7, pp. 543–557, Sept. 1995.

[9] L. Griffin, A. Colchester, and G. Robinson, "Scale and Segmentation of Grey-Level Images Using Maximum Gradient Paths," *Image and Vision Computing*, vol. 10, no. 6, pp. 389–402, July 1992.

[10] R. Haralick, "Ridges and Valleys on Digital Images," *Computer Vision, Graphics, and Image Processing*, vol. 22, no. 10, pp. 28–38, Apr. 1983.

[11] B. Jähne, "Spatio-Temporal Image Processing," Lecture Notes in Computer Science vol. 751, ch. 8, pp. 143–152, Springer-Verlag, 1993.

[12] M. Jordan, "Nouvelles Observations sur les lignes de faîte et de thalweg. *Comptes Rendus des Séances de l'ac. des sc.*, vol. 75, pp. 1,023–1,025, 1872.

[13] J. Koenderink and A. van Doorn, "Local Features of Smooth Shapes: Ridges and Courses," *Geometric Methods in Computer Vision II*, vol. 2,031, pp. 2–13. SPIE, 1993.

[14] D. Lloret, A. López, and J. Serrat, "Precise Registration of CT and MR Volumes Based on a New Creaseness Measure," *Noblesse Workshop on Non-Linear Model Based Image Analysis*, pp. 15–20. London: Springer-Verlag, 1998.

[15] A. López, D. Lloret, and J. Serrat, "Multilocal Creaseness Based on the Level Set Extrinsic Curvature," Technical Report 26, Centre de Visió per Computador, Dept. d'Informàtica, Universitat Autònoma de Barcelona, Spain, 1997.

[16] A. López, F. Lumbreras, and J. Serrat, "Creaseness from Level Set Extrinsic Curvature," H. Burkhardt and B. Neumann, eds., *Proc. Fifth European Conf. Computer Vision*, Lecture Notes in Computer Science vol. 1,407, pp. 156–169, Springer-Verlag, 1998.

[17] F. Lumbreras and J. Serrat, "Wavelet Filtering for the Segmentation of Marble Images," *Optical Eng.*, vol. 35, no. 10, pp. 2,864–2,872, Oct. 1996.

[18] J. Maintz, P. van den Elsen, and M. Viergever, "Evaluation of Ridge Seeking Operators for Multimodality Medical Image Matching," *IEEE Trans. Pattern Analysis and Machine Intelligence*, vol. 18, no. 4, pp. 353–365, Apr. 1996.

[19] J. Maxwell, "On Hills and Dales," *The London, Edinburgh and Dublin Philosophical Magazine and J. Science*, vol. 40, no. 269, pp. 421–425, 1870.

[20] L. Nackman, "Two-Dimensional Critical Point Configuration Graphs," *IEEE Trans. Pattern Analysis and Machine Intelligence*, vol. 6, no. 4, pp. 442–450, July 1984.

[21] L. Najman and M. Schmitt, "Watersheds of a Continuous Function," *Signal Processing*, vol. 38, no. 1, pp. 99–112, July 1994.

[22] J. O'Callaghan and D. Mark, "The Extraction of Drainage Networks from Digital Elevation Data," *Computer Vision, Graphics, and Image Processing*, vol. 28, no. 3, pp. 323–344, Dec. 1984.

[23] S. Pizer, D. Eberly, and D. Fritsch, "Zoom-Invariant Vision of Figural Shape: The Mathematics of Cores," *Computer Vision and Image Understanding*, vol. 69, no. 1, pp. 55–71, Jan. 1998.

[24] J. Rieger, "Topographical Properties of Generic Images," *Int'l J. Computer Vision*, vol. 23, no. 1, pp. 79–92, May 1997.

[25] P. Rosin, "Early Image Representation by Slope Districts," *J. Visual Comm. and Image Representation*, vol. 6, no. 3, pp. 228–243, Sept. 1995.

[26] R. Rothe, "Zum problem des talwegs," *Sitzungsberichte der Berliner Math. Gesellschaft*, vol. 14, pp. 51–69, 1915.

[27] P. Soille and C. Gratin, "An Efficient Algorithm for Drainage Network Extraction on DEMs," *J. Visual Comm. and Image Representation*, vol. 5. no. 2, pp. 181–189, June 1994.

[28] C. Steger, "An Unbiased Detector of Curvilinear Structures," *IEEE Trans. Pattern Analysis and Machine Intelligence*, vol. 20, no. 2, pp. 113–125, Feb. 1998.

[29] J.P. Thirion and A. Gourdon, "Computing the Differential Characteristics of Isointensity Surfaces," *Computer Vision, Graphics, and Image Processing: Image Understanding*, vol. 61, no. 2, pp. 190–202, Mar. 1995.

[30] L. Vincent and P. Soille, "Watersheds in Digital Spaces: An Efficient Algorithm Based on Immersion Simulations," *IEEE Trans. Pattern Analysis and Machine Intelligence*, vol. 13, no. 6, pp. 583–598, June 1991.

Antonio M. López received the BSc degree in computer science from the Universitat Politècnica de Catalunya in 1992 and the MSc degree in image processing and artificial intelligence from the Universitat Autònoma de Barcelona in 1994. Presently, he is an associate professor in the Computer Science Department at the Universitat Autònoma de Barcelona and is responsible for the area of technological development in the Centre de Visió per Computador (CVC). He is currently finishing his studies toward acquiring the PhD degree, which is devoted to the design and implementation of specific ridge and valley detectors with application to medical image analysis problems and drainage pattern delineation.

Felipe Lumbreras received the BSc degree in physics from the Universitat de Barcelona in 1991 and the MSc degree in computer science from the Universitat Autònoma de Barcelona in 1993. He is currently an associate professor in the Computer Science Department at the Universitat Autònoma de Barcelona, and a research member of the Centre de Visió per Computador (CVC). His research interests, in order to obtain his PhD degree, include wavelets and texture analysis. In addition, he participates in the development of machine vision applications for the industry.

Joan Serrat received his BSc degree in computer science from the Universitat Autònoma de Barcelona in 1986 and his PhD degree in computer science from the Universitat Autònoma de Barcelona in 1990. Presently, he is an associate professor in the Computer Science Department and a member of the Centre de Visió per Computador (CVC). His research interests are multisensor medical image registration and wavelets for texture analysis. In addition, he participates in the development of machine vision applications for the industry.

Juan J. Villanueva received his BSc degree in physics from the Universitat de Barcelona in 1973 and the PhD degree in computer science from the Universitat Autònoma de Barcelona in 1981. Since 1975, he has been teaching in the Computer Science Department at the Universitat Autònoma de Barcelona, where he was appointed professor in 1990. In 1986, Dr. Villanueva promoted the Centre de Visió per Computador (CVC) and has been its director since its inception. He was cofounder and vice president of AERFAI, which is the Spanish chapter of IAPR; he is currently a member of its steering committee. His research interests comprise all aspects of computer vision, in particular recognition based on geometrical models and medical computer vision applications. Dr. Villanueva is a member of the IEEE, SPIE, and the IEEE Computer Society.